

First Axion Results from the XENON100 Experiment

E. Aprile,¹ F. Agostini,² M. Alfonsi,³ K. Arisaka,⁴ F. Arneodo,^{5,*} M. Auger,⁶ C. Balan,⁷ P. Barrow,⁶ L. Baudis,⁶ B. Bauermeister,⁸ A. Behrens,⁶ P. Beltrame,^{9,†} K. Bokeloh,¹⁰ A. Brown,¹¹ E. Brown,¹⁰ S. Bruenner,¹² G. Bruno,⁵ R. Budnik,⁹ J. M. R. Cardoso,⁷ A. P. Colijn,³ H. Contreras,¹ J. P. Cussonneau,¹³ M. P. Decowski,³ E. Duchovni,⁹ S. Fattori,⁸ A. D. Ferella,⁵ W. Fulgione,¹⁴ F. Gao,¹⁵ M. Garbini,² C. Geis,⁸ L. W. Goetzke,¹ C. Grignon,⁸ E. Gross,⁹ W. Hampel,¹² R. Itay,⁹ F. Kaether,¹² G. Kessler,⁶ A. Kish,⁶ H. Landsman,⁹ R. F. Lang,¹¹ M. Le Calloch,¹³ D. Lellouch,⁹ C. Levy,¹⁰ S. Lindemann,¹² M. Lindner,¹² J. A. M. Lopes,⁷ K. Lung,⁴ A. Lyashenko,⁴ S. Macmullin,¹¹ T. Marrodán Undagoitia,¹² J. Masbou,¹³ F. V. Massoli,² D. Mayani Paras,⁶ A. J. Melgarejo Fernandez,¹ Y. Meng,⁴ M. Messina,¹ B. Miguez,¹⁴ A. Molinario,¹⁴ M. Murra,¹⁰ J. Naganoma,¹⁶ U. Oberlack,⁸ S. E. A. Orrigo,^{7,‡} E. Pantic,⁴ R. Persiani,² F. Piastra,⁶ J. Pienaar,¹¹ G. Plante,¹ N. Priel,^{9,§} S. Reichard,¹¹ C. Reuter,¹¹ A. Rizzo,¹ S. Rosendahl,¹⁰ J. M. F. dos Santos,⁷ G. Sartorelli,² S. Schindler,⁸ J. Schreiner,¹² M. Schumann,¹⁷ L. Scotto Lavina,¹³ M. Selvi,² P. Shagin,¹⁶ H. Simgen,¹² A. Teymourian,⁴ D. Thers,¹³ A. Tiseni,³ G. Trincheri,¹⁴ O. Vitells,⁹ H. Wang,⁴ M. Weber,¹² and C. Weinheimer.¹⁰

(The XENON100 Collaboration)

¹Physics Department, Columbia University, New York, NY, USA

²University of Bologna and INFN-Bologna, Bologna, Italy

³Nikhef and the University of Amsterdam, Science Park, Amsterdam, Netherlands

⁴Physics & Astronomy Department, University of California, Los Angeles, CA, USA

⁵INFN, Laboratori Nazionali del Gran Sasso, Assergi (AQ), Italy

⁶Physics Institute, University of Zürich, Zürich, Switzerland

⁷Department of Physics, University of Coimbra, Coimbra, Portugal

⁸Institut für Physik & Exzellenzcluster PRISMA, Johannes Gutenberg-Universität Mainz, Mainz, Germany

⁹Department of Particle Physics and Astrophysics, Weizmann Institute of Science, Rehovot, Israel

¹⁰Institut für Kernphysik, Wilhelms-Universität Münster, Münster, Germany

¹¹Department of Physics, Purdue University, West Lafayette, IN, USA

¹²Max-Planck-Institut für Kernphysik, Heidelberg, Germany

¹³SUBATECH, Ecole des Mines de Nantes, CNRS/In2p3, Université de Nantes, Nantes, France

¹⁴INFN-Torino and Osservatorio Astrofisico di Torino, Torino, Italy

¹⁵Department of Physics & Astronomy, Shanghai Jiao Tong University, Shanghai, China

¹⁶Department of Physics and Astronomy, Rice University, Houston, TX, USA

¹⁷Albert Einstein Center for Fundamental Physics, University of Bern, Bern, Switzerland

We present the first results of searches for axions and axion-like-particles with the XENON100 experiment. The axion-electron coupling constant, g_{Ae} , has been tested by exploiting the axio-electric effect in liquid xenon. A profile likelihood analysis of 224.6 live days \times 34 kg exposure has shown no evidence for a signal. By rejecting g_{Ae} larger than 7.7×10^{-12} (90% CL) in the solar axion search, we set the best limit to date on this coupling. In the frame of the DFSZ and KSVZ models, we exclude QCD axions heavier than 0.3 eV/ c^2 and 80 eV/ c^2 , respectively. For axion-like-particles, under the assumption that they constitute the whole abundance of dark matter in our galaxy, we constrain g_{Ae} to be lower than 1×10^{-12} (90% CL) for masses between 5 and 10 keV/ c^2 .

PACS numbers:

Keywords: Dark Matter, Axion, Xenon

I. INTRODUCTION

Axions were introduced in the Peccei-Quinn solution of the strong CP problem as pseudo-Nambu-Goldstone bosons emerging from the breaking of a global U(1) sym-

metry [1–3]. Although this original model has been ruled out, “invisible” axions (arising from a higher symmetry-breaking energy scale) are still allowed, as described, for example, in the DFSZ and KSVZ models [4–7]. In addition to QCD axions, axion-like particles (ALPs) are pseudoscalars that do not necessarily solve the strong CP problem, but which have been introduced by many extensions of the Standard Model of particle physics. Axions as well as ALPs are well motivated cold dark matter candidates [8].

Astrophysical observations are thought to be the most sensitive technique for detecting axions and ALPs [9]: the Sun would constitute an intense source of axions and ALPs, where they can be pro-

*Present address: New York University in Abu Dhabi, UAE.

†Present address: School of Physics & Astronomy, The University of Edinburgh, Edinburgh, United Kingdom.; Electronic address: paolo.beltrame@ed.ac.uk

‡Present address: IFIC, CSIC-Universidad de Valencia, Valencia, Spain.

§Electronic address: nadav.priel@weizmann.ac.il

duced via Bremsstrahlung, Compton scattering, axio-recombination and axio-deexcitation [10] (referred to as solar axions). Additionally, searches can be conducted for ALPs that may have been generated via a non-thermal production mechanism in the early universe and which now constitute the dark matter in our galaxy (referred to as galactic ALPs).

Axions and ALPs may give rise to observable signatures in detectors through their coupling to photons ($g_{A\gamma}$), electrons (g_{Ae}) and nuclei (g_{AN}). The coupling g_{Ae} may be tested via scattering off the electron of a target, such as liquid xenon (LXe), through the axio-electric effect [11–15]. This process is the analogue of the photo-electric effect with the absorption of an axion instead of a photon.

We report on the first axion searches performed with the XENON100 detector. The expected interaction rate is obtained by the convolution of the flux and the axio-electric cross section. The latter is given, both for QCD axions and ALPs, by

$$\sigma_{Ae} = \sigma_{pe}(E_A) \frac{g_{Ae}^2}{\beta_A} \frac{3E_A^2}{16\pi \alpha_{em} m_e^2} \left(1 - \frac{\beta_A^{2/3}}{3}\right), \quad (1)$$

as described in [12–16]. In Eq. 1, σ_{pe} is the photoelectric cross section for LXe [17], E_A is the axion energy, α_{em} is the fine structure constant, m_e is the electron mass, and β_A is the axion velocity over the speed of light, c .

The solar axion flux has recently been recalculated in [10]. This incorporates four production mechanisms that depend upon g_{Ae} : Bremsstrahlung, Compton scattering, atomic recombination, and atomic deexcitation. The corresponding flux is 30% larger than previous estimates due to atomic recombination and deexcitation, which were not previously taken into account. However, [10] does not include corrections for axions with a mass larger than 1 keV/ c^2 , which constitutes an upper mass limit for our analysis. For solar axions, both flux and cross-section depend upon g_{Ae}^2 , thus the interaction rate scales with the fourth power of the axion-electron coupling.

For non-relativistic ALPs in the galaxy, assuming that they constitute the whole dark matter halo density ($\rho_{DM} \sim 0.3$ GeV/cm³ [18]), the total flux is given by $\phi_{ALP} = c\beta_A \times \rho_{DM}/m_A$, where m_A is the ALP mass. The interaction rate for these ALPs depends on g_{Ae}^2 , as the flux is independent from the axion coupling. As $\beta_A \approx 10^{-3}$ in the non-relativistic regime, the velocities cancel out in the convolution between σ_{Ae} and the flux. Thus the expected electron recoil spectrum is independent from the particle speed. As the kinetic energy of the ALPs is negligible with respect to their rest mass energy, a monoenergetic peak at the axion mass is expected in the spectrum.

II. ANALYSIS

A. XENON100

The XENON100 detector is a double-phase time projection chamber with a LXe target operating at the Laboratori Nazionali del Gran Sasso (LNGS) in Italy. A total of 178 low radioactivity, UV-sensitive photomultiplier tubes (PMTs) measure signals induced by particles interacting in the sensitive volume, which contains 62 kg of ultra-pure LXe. An energy deposition in the detector produces both scintillation photons and ionization electrons. The electrons, moved from the interaction point by a drift field of 530 V/cm, are extracted from the liquid and accelerated in the gas by a 12 kV/cm field, producing proportional scintillation light. The direct scintillation signal ($S1$) and the amplified charge signal ($S2$) are detected by the PMTs. The time difference between the $S1$ and the $S2$ signals is used to estimate the z-coordinate of the interaction, while the $S2$ -hit-pattern on the PMTs is employed to estimate the (x, y)-coordinate. A detailed description of the instrument and its operational principle is given in [19].

The XENON100 detector is installed at LNGS, at an average depth of 3600 m water equivalent, where the muon flux is suppressed by six orders of magnitude with respect to sea level. Due to a careful selection of materials, the total background in the inner 34 kg fiducial volume is 5.3×10^{-3} events/(keV \times kg \times day) [20, 21]. This ultra low background makes XENON100 sensitive to rare event searches in general, and in particular for those producing electronic recoils (ER), as is the case for axions.

B. Data sample and analysis

In this work, we analyse the same data set used for the spin-independent [20] and spin-dependent [22] WIMP-searches, with an exposure of 224.6 live days and 34 kg fiducial mass. Detailed information on the analysis procedure is available in [23]. The same quality and selection cuts are applied, with the exception of a consistency cut on the $S2$ width, which was found to be not useful for this ER analysis.

Fig. 1 (top) shows the distribution in the $\log_{10}(S2_b/S1)$ vs. $S1$ for calibration data (grey dots), and the science data passing all the selection cuts (black dots), where only the $S2$ signal detected by the bottom PMTs, $S2_b$, is used since it requires smaller corrections [19]. The calibration data is obtained by exposing the detector to ⁶⁰Co and ²³²Th sources. The mean of the $\log_{10}(S2_b/S1)$ band from the calibration is subtracted in order to remove the energy-dependence of this parameter. The lower energy threshold was set to 3 photoelectrons (PE) in $S1$ in order to limit the presence of random coincidences from dark counts in the PMTs. In addition, a lower threshold of 150 PE in $S2$ has been imposed to be unaffected by the trigger threshold [23]. In order to reject ER events with

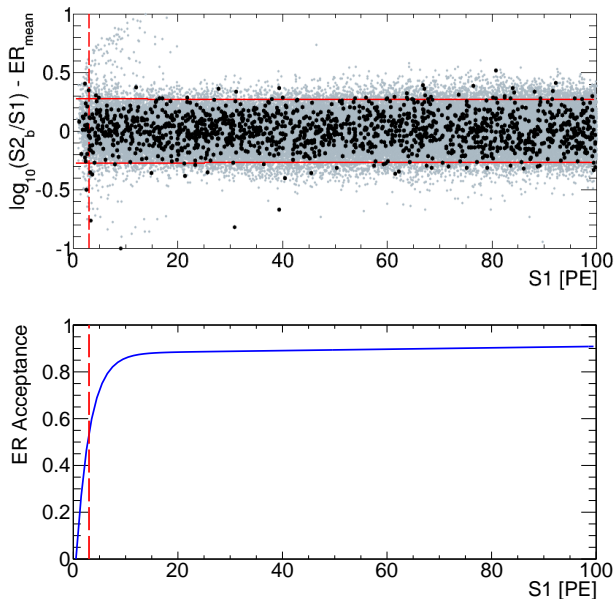


FIG. 1: *Top*: Event distribution in the flattened $\log_{10}(S2_b/S1)$ vs. $S1$ space for science data (black points) and calibration (grey points). Straight dashed lines show the selection cut on the flattened $\log_{10}(S2_b/S1)$ (horizontal red lines) and the 3 PE threshold cut (red vertical line). *Bottom*: Global acceptance for electronic recoil events, evaluated on calibration data.

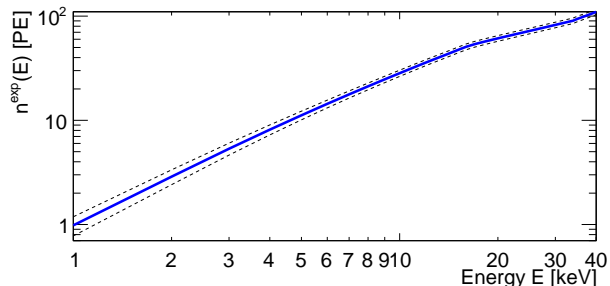


FIG. 2: Conversion function between energy recoil in keV and $S1$ in PE. The n^{exp} central value and the $\pm 1\sigma$ uncertainty are indicated with solid blue and black dashed line, respectively.

an anomalously high or low $S2/S1$ ratio, signal candidates are required to be inside the 2σ band around the $\log_{10}(S2_b/S1)$ median [23]. This is shown by the horizontal red dashed lines in Fig.1 (top). The combined acceptance of all selection cuts for ER events is evaluated on calibration data, and is shown in Fig.1 (bottom). Upper thresholds of 30 and 100 PE were employed for the axions from the Sun and the non-relativistic ALPs searches, respectively.

The energy deposited by each interaction is computed in this analysis using the $S1$ signal. This is converted into an electronic recoil energy E , by taking into account the scintillation efficiency $R(E)$ relative to 32.1 keV (measured at zero-field by [24] and [25]), and the quenching

factor $Q(E)$ at a non-zero electric field (measured at a field close to the one of XENON100 [25]). The NEST model (v0.98) [26] is employed to estimate the energy for this study as it agrees within uncertainties with the measurements at zero field [24, 25], as well as the measurements with a non-zero field [25, 27]. The uncertainty on $R(E) \times Q(E)$ is taken from NEST and assumed to be Gaussian. This reflects the intrinsic uncertainty of the model (4%) as well as the spread in the measured data points, particularly relevant at low energies. The conversion from the energy deposition E to the observed signal n^{exp} in PE is therefore given by

$$n^{exp}(E) = R(E) \times Q(E) \times f \times E \equiv L_Y(E) \times E, \quad (2)$$

where the factor $f = 3.76$ PE/keV is the derived XENON100 light yield at 32.1 keV and zero field [19, 27]. The conversion function $n^{exp}(E)$ is shown in Fig.2, together with the $\pm 1\sigma$ uncertainty. The final results on g_{Ae} are robust against changes in the energy scale: if $L_Y(E)$ is varied by 25%, the limits change by less than 5% for the solar and about 10% for the galactic axion searches.

C. Statistical method

A Profile Likelihood analysis, as described in [28] and analogous to [29], is used to constrain the coupling constant g_{Ae} . The full likelihood function is given by

$$\mathcal{L} = \mathcal{L}_1(g_{Ae}, N_b, n^{exp}) \times \mathcal{L}_2(n^{exp}), \quad (3)$$

where N_b is the number of expected background events. The parameter of interest is g_{Ae} , whereas N_b and n^{exp} are considered as nuisance parameters.

The signal likelihood function, \mathcal{L}_1 , is given by

$$\mathcal{L}_1 = \text{Poiss}(N|N_s + N_b) \prod_{i=1}^N \frac{N_s f_s(S1_i) + N_b f_b(S1_i)}{N_s + N_b}, \quad (4)$$

where N_s and N_b are the expected number of signal and background events in the signal region, and N_s depends upon g_{Ae} and n^{exp} . N is the total number of observed events, and the $S1_i$ corresponds to the $S1$ of the i -th event. The functions f_s and f_b are the signal and background normalized p.d.f. spectra.

The event rate with a given number of detected photons, n , is obtained by applying Poisson smearing to the predicted energy spectrum dR/dE ,

$$\frac{dR}{dn} = \int_0^\infty \frac{dR}{dE} \times \text{Poiss}(n|n^{exp}(E)) dE, \quad (5)$$

where n^{exp} is obtained from Eq.2.

Then the rate as a function of the measured number of photoelectrons, $S1$, is given by

$$\frac{dR}{dS1} = \sum_{n=1}^\infty \text{Gauss}(S1|n, \sqrt{n}\sigma_{PMT}) \times \frac{dR}{dn} \times \epsilon(S1), \quad (6)$$

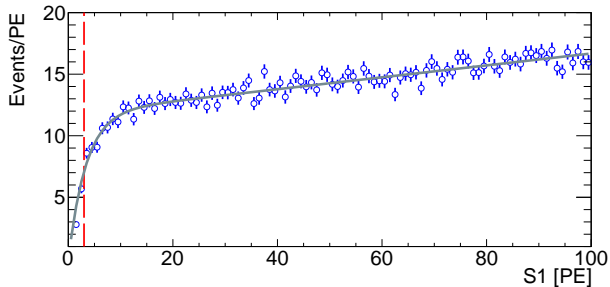


FIG. 3: Background model $N_b \times f_b$ (grey line), scaled to the correct exposure, as explained in the text. f_b is based on the ^{60}Co and ^{232}Th calibration data (empty blue dots), and is used in Eq.4. The 3 PE threshold is indicated by the vertical red dashed line.

where $\epsilon(S1)$ is the acceptance and $\sigma_{PMT} = 0.5$ PE is the PMT resolution [23].

The background spectrum, f_b , is modeled based on ^{60}Co and ^{232}Th calibration data. The spectrum is scaled to the science data exposure by normalizing it to the number of events seen outside the signal region. For solar axions, it is done between 30 and 100 PE, and for galactic ALPs below $m_A[\text{pe}] - 2\sigma$ and above $m_A[\text{pe}] + 2\sigma$, where $m_A[\text{pe}]$ is the ALP mass in units of PE and σ is the width of the expected signal peak, see Fig.6. Then, the scaled background spectrum is integrated in the signal region to give the expected number of background events, N_b . The background model scaled to the correct exposure, $N_b \times f_b$, is shown in Fig.3, along with the scaled calibration spectrum.

The energy scale term in Eq.3, \mathcal{L}_2 , has been parametrised with a single nuisance parameter t . The likelihood function is defined to be normally distributed with zero mean and unit variance, corresponding to

$$\mathcal{L}_2(n^{exp}(t)) = e^{-t^2/2}, \quad (7)$$

where $t = \pm 1$ corresponds to a $\pm 1\sigma$ deviation in n^{exp} , as shown in Fig.2, *i.e.*, $t = (n^{exp} - n_{mean}^{exp})/\sigma$.

III. RESULTS

A. Solar axions

The remaining events after all the selection cuts are shown in Fig.4 as a function of $S1$. The solid grey line shows the background model, $N_b \times f_b$. The expected $S1$ spectrum for solar axions, lighter than $1 \text{ keV}/c^2$, is shown as a blue dashed line for $g_{Ae} = 2 \times 10^{-11}$, the best limit so far reported by the EDELWEISS-II collaboration [30]. The data are compatible with the background model, and no excess is observed for the background only hypothesis.

Fig.5 shows the new XENON100 exclusion limit on g_{Ae} at 90% CL. The sensitivity is shown by the green/yellow band ($1\sigma/2\sigma$). As we used the most recent and accurate

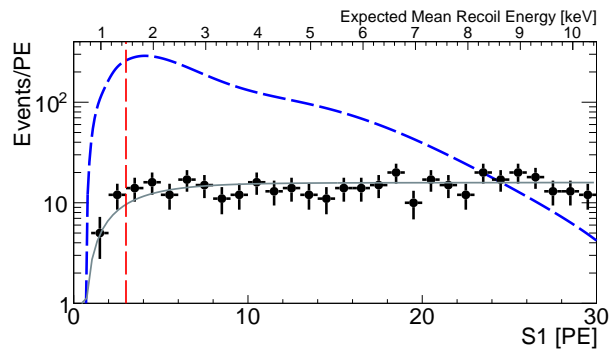


FIG. 4: Event distribution of the data (black dots), and background model (grey) of the solar axion search. The expected signal for solar axions with $m_A < 1 \text{ keV}/c^2$ is shown by the dashed blue line, assuming $g_{Ae} = 2 \times 10^{-11}$, the current best limit from EDELWEISS-II [30]. The vertical dashed red line indicates the low $S1$ threshold, set at 3 PE. The top axis shows the expected mean value of the electronic recoil energy.

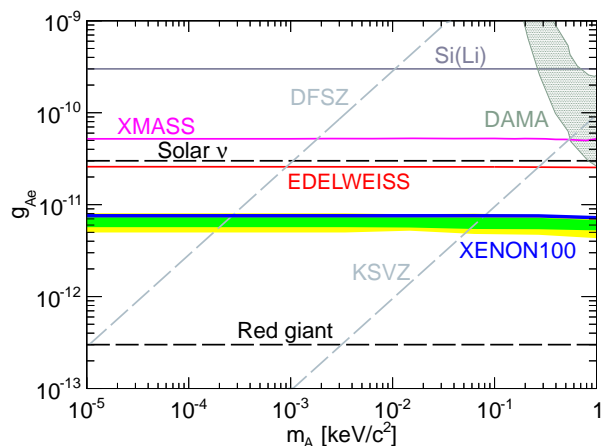


FIG. 5: The XENON100 limits (90% CL) on solar axions is indicated by the blue line. The expected sensitivity is given by the green/yellow bands ($1\sigma/2\sigma$). Limits by EDELWEISS-II [30], and XMASS [31] are shown, together with the limits from a Si(Li) detector from Derbin et al. [32]. The contour area corresponds to a possible interpretation of the DAMA/LIBRA annual modulation signal as originating from axions [33]. Indirect astrophysical bounds from solar neutrinos [34] and red giants [35] are represented by dashed lines. The benchmark DFSZ and KSVZ models are represented by grey dashed lines [4–7].

calculation for solar axion flux from [10], which is valid only for light axions, we restrict the search to $m_A < 1 \text{ keV}/c^2$. For comparison, we also present recent experimental constraints [30–32] and the DAMA/LIBRA annual modulation signal [33] interpreted as being due to axion interactions. Astrophysical bounds [34, 35] and theoretical benchmark models [4–7] are also shown. For solar axions with masses below $1 \text{ keV}/c^2$ XENON100 is able to set the strongest constraint on the coupling to electrons, excluding values of g_{Ae} larger than 7.7×10^{-12}

(90% CL).

For a specific axion model, the limit on the dimensionless coupling g_{Ae} translates to a limit on the axion mass. Within the DFSZ and KSVZ models [4–7] XENON100 excludes axion masses above $0.3 \text{ eV}/c^2$ and $80 \text{ eV}/c^2$, respectively. For comparison, the CAST experiment, testing the coupling to photons, $g_{A\gamma}$, has excluded axions within the KSVZ model in the mass range between $0.64 - 1.17 \text{ eV}/c^2$ [36].

B. Galactic axions-like particles

For non-relativistic galactic ALPs, Fig.6 shows the XENON100 data after the selection cuts along with their statistical errors, together with the expected signal for different masses. A coupling of $g_{Ae} = 4 \times 10^{-12}$ and the condition that ALPs constitute all of the galactic dark matter have been assumed. The width of the monoenergetic signal is given by the energy resolution of the detector at the relevant $S1$ [19]. As for the solar axion search, the data is compatible with the background model, and no excess is observed for the background-only hypothesis for the various ALP masses.

Fig.7 shows the XENON100 90% CL exclusion limit. As downward statistical fluctuations of the background might lead to reject couplings to which the experiment is not sensitive, we used the CL_s method to protect the result from this effect, as described in [29]. The XENON100 result is shown compared to other experimental constraints [30, 37, 38] and to the DAMA/LIBRA annual modulation interpretation [33]. Astrophysical bounds [34, 35] and a theoretical benchmark model [6, 7] are also presented. The expected sensitivity is shown by the green/yellow bands ($1\sigma/2\sigma$). The steps in the sensitivity around 5 and 35 keV/c^2 reflect the photoelectric cross section due to the atomic energy levels. Below 5 keV/c^2 the obtained 90% CL is higher than expected deviating by as much as 2σ from the mean predicted sensitivity. This is due to a slight excess of events between 3 and 5 PE. A similar effect is responsible for the limit oscillating around the predicted sensitivity above 5 keV/c^2 . The ALPs limit is very sensitive to fluctuations in individual bins because of the expected monoenergetic signal. In the 5-10 keV/c^2 mass range, XENON100 sets the best upper limit, excluding an axion-electron coupling $g_{Ae} > 1 \times 10^{-12}$ at the 90% CL, assuming that ALPs constitute all of the galactic dark matter.

IV. ACKNOWLEDGMENTS

We gratefully acknowledge support from NSF, DOE, SNF, Volkswagen Foundation, FCT, Region des Pays de la Loire, STCSM, NSFC, DFG, MPG, Stichting voor Fundamenteel Onderzoek der Materie (FOM), the Weizmann Institute of Science, the EMG research center and

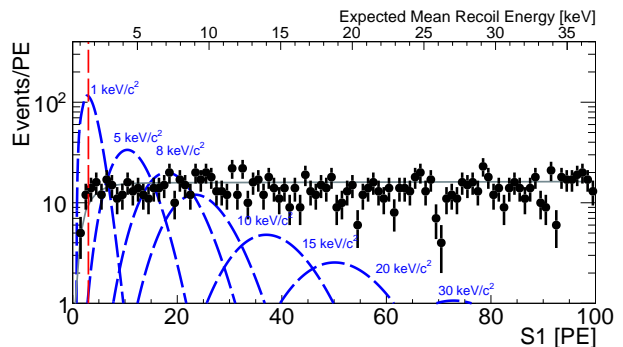


FIG. 6: Event distribution in the galactic ALPs search region between 3 and 100 PE (black dots). The grey line shows the background model used for the profile likelihood function. The red dashed line indicates the $S1$ threshold. The expected signal in XENON100 for various ALP masses, assuming $g_{Ae} = 4 \times 10^{-12}$ is shown as blue dashed lines. The top axis shows the expected mean electronic recoil energy value.

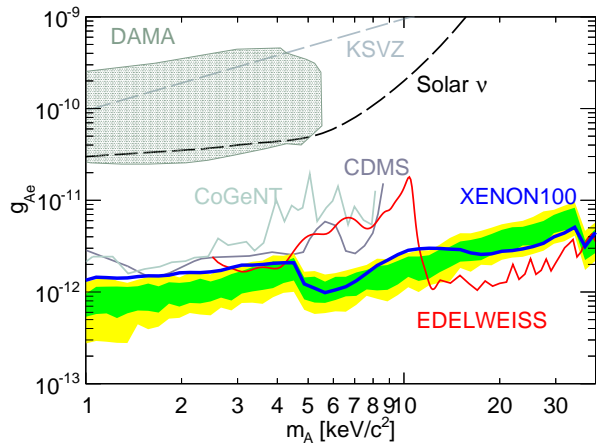


FIG. 7: The XENON100 limit (90% CL) on ALP coupling to electrons as a function of the mass, under the assumption that ALPs constitute all the dark matter in our galaxy (blue line). The expected sensitivity is shown by the green/yellow bands ($1\sigma/2\sigma$). The contour area corresponds to a possible interpretation of the DAMA annual modulation signal [33] as ALP interaction, while the other curves are constraints set by CoGeNT [37] (brown dashed line), CDMS [38] (grey continuous line), and EDELWEISS-II [30] (red line, extending up to 40 keV/c^2). Indirect astrophysical bound from solar neutrinos [34] is represented as a dashed line. The benchmark KSVZ model is represented by a dashed grey line [6, 7].

INFN. We are grateful to LNGS for hosting and supporting XENON100.

-
- [1] R. D. Peccei and H. R. Quinn, Phys. Rev. Lett. **1440**, 38 (1977).
- [2] S. Weinberg, Phys. Rev. Lett. **40**, 223 (1978).
- [3] F. Wilczek, Phys. Rev. Lett. **40**, 279 (1978).
- [4] M. Dine, W. Fischler, and M. Srednicki, Phys. Lett B **104**, 199 (1981).
- [5] A. R. Zhitnitsky, Sov. J. Nucl. Phys. **31**, 260 (1980).
- [6] J. E. Kim, Phys. Rev. Lett. **43**, 103 (1979).
- [7] M. A. Shifman, A. I. Vainshtein, and V. I. Zakharov, Nucl. Phys. B **166**, 493 (1980).
- [8] L. Abbott and P. Sikivie, Phys. Lett. **B120**, 133 (1983).
- [9] P. Sikivie, Phys. Rev. Lett. **51**, 1415 (1983).
- [10] J. Redondo (2013), arXiv:1310.0823.
- [11] S. Dimopoulos, G. D. Starkman, and B. W. Lynn, Phys. Rev. B **168**, 145 (1986).
- [12] F. T. Avignone et al., Phys. Rev. D **35**, 2752 (1987).
- [13] M. Pospelov, A. Ritz, and M. Voloshin, Phys. Rev. D **78**, 115012 (2008).
- [14] A. Derevianko et al., Phys. Rev. D **82**, 065006 (2010).
- [15] K. Arisaka et al., Astropart. Phys. **44**, 59 (2013).
- [16] F. Alessandria et al. (CUORE Coll.), JCAP **1305**, 007 (2013).
- [17] NIST, URL <http://physics.nist.gov/PhysRefData/Xcom/html/xcom1.html>.
- [18] A. M. Green, Mod. Phys. Lett. **A27**, 1230004 (2012).
- [19] E. Aprile et al. (XENON100 Coll.), Astropart. Phys. **35**, 573 (2012).
- [20] E. Aprile et al. (XENON100 Coll.), Phys. Rev. Lett. **109**, 181301 (2012).
- [21] E. Aprile et al. (XENON100 Coll.), Phys. Rev. D **83**, 082001 (2011).
- [22] E. Aprile et al. (XENON100 Coll.), Phys. Rev. Lett. **111**, 021301 (2013).
- [23] E. Aprile et al. (XENON100 Coll.), Astropart. Phys. **11**, 54 (2014).
- [24] E. Aprile et al., Phys. Rev. D **86**, 112004 (2012).
- [25] L. Baudis et al., Phys. Rev. D **87**, 115015 (2013).
- [26] M. Szydagis et al., JINST **6**, 10002 (2011).
- [27] A. Manalaysay et al., Rev. Sci. Instrum. **81**, 073303 (2010).
- [28] G. Cowan et al., Eur.Phys.J. **C71**, 1554 (2011).
- [29] E. Aprile et al. (XENON100 Coll.), Phys. Rev. D **84**, 052003 (2011).
- [30] E. Armengaud et al. (EDELWEISS-II Coll.), JCAP **1311**, 067 (2013).
- [31] K. Abe et al. (XMASS Coll.), Phys. Lett. B **724**, 46 (2013).
- [32] A. Derbin et al., JETP Lett. **95**, 339 (2012).
- [33] R. Bernabei et al. (DAMA Coll.), Int. J. Mod. Phys. A **21**, 1445 (2006).
- [34] P. Gondolo and G. G. Raffelt, Phys. Rev. D **79**, 107301 (2009).
- [35] G. G. Raffelt, Lect. Notes Phys. **741**, 51 (2008).
- [36] M. Arik et al. (CAST Coll.), Phys. Rev. Lett. **112**, 091302 (2014).
- [37] C. E. Aalseth et al. (CoGeNT Coll.), Phys. Rev. Lett. **101**, 251301 (2008).
- [38] Z. Ahmed et al. (CDMS Coll.), Phys. Rev. Lett. **103**, 141802 (2009).